The dynamic compensation temperature in a kinetic spin-5/2 Ising model on a hexagonal lattice

Ümüt Temizer[a)†] and Ayşegül Özkılıç[b)]

[a)] *Department of Physics, Bozok University, 66200 Yozgat, Turkey*
[b)] *Institute of Science, Bozok University, 66200 Yozgat, Turkey*

(Received 2 August 2012)

We present a study of the dynamic behavior of a two-sublattice spin-5/2 Ising model with bilinear and crystal-field interactions in the presence of a time-dependent oscillating external magnetic field on alternating layers of a hexagonal lattice by using the Glauber-type stochastic dynamics. The lattice is formed by alternate layers of spins $\sigma = 5/2$ and $S = 5/2$. We employ the Glauber transition rates to construct the mean-field dynamic equations. First, we investigate the time variations of the average sublattice magnetizations to find the phases in the system and then the thermal behavior of the dynamic sublattice magnetizations to characterize the nature (first- or second-order) of the phase transitions and to obtain the dynamic phase transition (DPT) points. We also study the thermal behavior of the dynamic total magnetization to find the dynamic compensation temperature and to determine the type of the dynamic compensation behavior. We present the dynamic phase diagrams, including the dynamic compensation temperatures, in nine different planes. The phase diagrams contain seven different fundamental phases, thirteen different mixed phases, in which the binary and ternary combination of fundamental phases and the compensation temperature or the *L*-type behavior strongly depend on the interaction parameters.

Keywords: kinetic Ising model, dynamic phase transition, dynamic compensation temperature

PACS: 75.10.Hk,74.40.Gh, 64.60.Ht, 75.30. Kz **DOI:** 10.1088/1674-1056/22/3/037501

1. Introduction

The compensation temperature is the temperature at which the total magnetization vanishes below the critical temperature.[1] The existence of the compensation temperature is due to the fact that the magnetic moments of sublattices compensate each other completely owing to different temperature dependences of the sublattice magnetizations. At the compensation temperature, since there is no net magnetization, the material cannot interact with external fields. Therefore, the coercivity is extremely high and has a peak at the compensation temperature favoring the creation of small, stable magnetic domains. The compensation point is of great technological importance, since at this point only a small driving field is required to change the sign of the total magnetization. This property is very useful in thermomagnetic recording, electronic, and computer technologies.[2–4]

The static compensation temperatures of mixed spin Ising systems have been studied by using a variety of techniques in equilibrium statistical physics, such as the mean-field approximation (MFA), the real-space renormalization-group (RG) approach, Monte–Carlo (MC) simulations, the effective-field theory (EFT), the numerical transfer-matrix technique, and the exact formulation on the Bethe lattice by using the exact recursion equations (see Refs. [5]–[23] and references therein). However, the presence of the dynamic compensation temperature in the mixed spin-1/2 and spin-1,[24–26] the mixed spin-1/2 and spin-3/2,[27] the mixed spin-3/2 and spin-5/2,[28] the mixed spin-1 and spin-3/2,[29] the mixed spin-2 and spin-5/2,[30] and the mixed spin-1 and spin-2[31] Ising systems have also been investigated.

On the other hand, the spin-5/2 Ising system is one of the most important systems that have been used for studying the thermodynamic behaviors of many cooperative physical systems. The equilibrium properties of the system have been studied by well known methods in equilibrium statistical physics.[32–41] Although considerable progresses have been made in understanding the equilibrium properties of the model, the nonequilibrium properties of the model have not been as thoroughly explored. There have been only a few investigations, to our knowledge, about the dynamical aspects of the model. Christianson *et al*.[42] studied the critical dynamics of a spin-5/2 two-dimensional isotropic antiferromagnet. Wildes *et al*.[43] presented a comprehensive study of the static and the dynamic critical properties of the quasi two-dimensional spin-5/2 antiferromagnet $MnPS_3$. Keskin and his co-workers[44,45] have investigated the nonequilibrium aspects of spin-5/2 Blume–Capel (BC)[44] and spin-5/2 Blume–Emery–Griffiths (BEG)[45] Ising systems by using the dynamic MFA based on the Glauber-type stochastic dynamics.[46] Recently, Ertaş *et al*.[47] studied the dynamics of the spin-5/2 BC model with a single-ion crystal field under a time-dependent oscillating external magnetic field by using the EFT with correlations based on the exact Van der Waerden identity. The aim of this paper is to study the existence of the dynamic compen-

†Corresponding author. E-mail: umut.temizer@bozok.edu.tr

© 2013 Chinese Physical Society and IOP Publishing Ltd

sation temperature in the kinetic spin-5/2 Ising model with bilinear and crystal-field interactions under a time-dependent oscillating external magnetic field on alternate layers of a hexagonal lattice by using the Glauber-type stochastic dynamics. This work is important because it is dealing the ferrimagnetism as well as the dynamic compensation temperature. For this purpose, firstly we examine the time variations in average sublattice magnetizations to find the phases in the system, and the thermal behavior of the average sublattice magnetizations in a period or the dynamic sublattice magnetizations to obtain the dynamic phase transition (DPT) points. Then, we investigate the dynamic total magnetization as a function of the temperature to find the dynamic compensation temperatures as well as to determine the type of the compensation behavior. From these studies, dynamic phase diagrams, including the dynamic compensation temperatures, are presented in nine different planes. Finally, it is worthwhile mentioning that the compensation temperatures have been observed experimentally in different systems.[48,49]

The rest of the paper is organized as follows. In Section 2, the model is presented briefly, and the derivation of the mean-field dynamic equations is given by using the Glauber-type stochastic dynamics in the presence of a time-dependent oscillating external magnetic field. In Section 3, the behaviors of the average sublattice magnetizations, the dynamic sublattice magnetizations, and the dynamic total magnetization are studied in detail, and dynamic phase diagrams are presented in different planes. Finally, we give the summary and conclusion.

2. Model and formulas

We consider a spin-5/2 Ising model on a hexagonal lattice under an oscillating magnetic field. The model consists of two interpenetrating sublattices with spin variables $\sigma = \pm 5/2, \pm 3/2, \pm 1/2$ and $S = \pm 5/2, \pm 3/2, \pm 1/2$ on sites of sublattices A and B, respectively. The σ spins occupy the sites of one sublattice, say sublattice A, and the S spins occupy the other sublattice, namely sublattice B. The σ and S spins are distributed on alternate layers of the hexagonal lattice as shown in Fig. 1. In this figure, open and solid circles represent σ and S spins, respectively. The Hamiltonian for this system reads

$$\begin{aligned}\mathscr{H} = & -J_1 \sum_{\langle ij \rangle} \sigma_i S_j - J_2 \sum_{\langle ij \rangle} \sigma_i \sigma_j - J_3 \sum_{\langle ij \rangle} S_i S_j \\ & - D\left(\sum_i \sigma_i^2 + \sum_j S_j^2 \right) - H\left(\sum_i \sigma_i + \sum_j S_j \right), \quad (1)\end{aligned}$$

where the summation index $\langle ij \rangle$ denotes the summation over all pairs of neighboring spins, J_1, J_2, and J_3 are the exchange couplings between the nearest-neighbor pairs of spins σ–S, σ–σ, and S–S, respectively. It is seen from Fig. 1 that the J_1 interaction is restricted to the z_1 nearest-neighbor pair of spins, $z_1 = 4$, J_2 and J_3 are restricted to the coordination numbers of z_2 and z_3, respectively, where $z_2 = z_3 = 2$. Hence, we consider that the interactions among spins on sublattices A and B are different, i.e., $J_2 \neq J_3$. The parameter J_1 will be taken to be negative in all the subsequent analyses, that is, the intersublattice coupling is antiferromagnetic. The D is the crystal-field interaction or a single-ion anisotropy constant, and H describes a time-dependent oscillating external magnetic field. The H is given by

$$H(t) = H_0 \cos(wt), \quad (2)$$

where H_0 and $w = 2\pi\nu$ are the amplitude and the angular frequency of the oscillating field, respectively. The system is in contact with an isothermal heat bath at absolute temperature T_{A}.

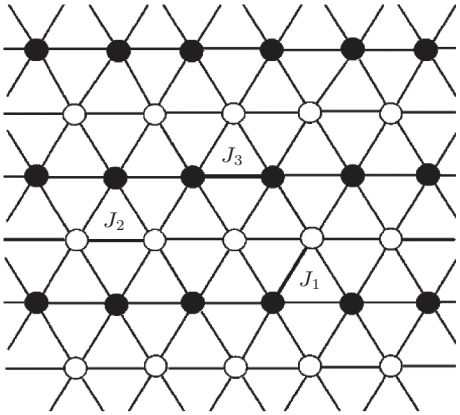


Fig. 1. Spin arrangement on the hexagonal lattice. The lattice is formed by alternate layers of σ (open circles) and S (solid circles) spins.

Now we apply the Glauber-type stochastic dynamics to obtain a set of mean-field dynamic equations. The system evolves according to a Glauber-type stochastic process at the transitional rate of $1/\tau$; hence the frequency of spin flipping, f, is $1/\tau$. Leaving the S spins on sublattice B fixed, we define $P^{\mathrm{A}}(\sigma_1, \sigma_2, \ldots, \sigma_N; t)$ as the probability that the system has the σ-spin configuration $\sigma_1, \sigma_2, \ldots, \sigma_N$ at time t. Similarly, leaving the σ spins on sublattice A fixed, we define $P^{\mathrm{B}}(S_1, S_2, \ldots, S_N; t)$ as the probability that the system has the S-spin configuration $S_1, S_2, \ldots, S_N$ at time t. Then, we calculate the probabilities that the i-th σ spin changes from value σ_i to σ_i' (with the S spins momentarily fixed) in an unit time $W_i^{\mathrm{A}}(\sigma_i \to \sigma_i')$ and the j-th S spin changes from value S_j to S_j' (with the σ spins momentarily fixed) in an unit time $W_j^{\mathrm{B}}(S_j \to S_j')$ respectively. Therefore, if the S spins on sublattice B are momentarily fixed, the master equation for the σ spins on sublattice A can be written as

$$\begin{aligned}& \frac{\mathrm{d}}{\mathrm{d}t} P^{\mathrm{A}}(\sigma_1, \sigma_2, \ldots, \sigma_N; t) \\ & = -\sum_i \left(\sum_{\sigma_i \neq \sigma_i'} W_i^{\mathrm{A}}(\sigma_i \to \sigma_i') \right) P^{\mathrm{A}}(\sigma_1, \sigma_2, \ldots, \sigma_i, \ldots, \sigma_N; t)\end{aligned}$$

$$+\sum_i\left(\sum_{\sigma_i\neq\sigma_i'}W_i^{\rm A}(\sigma_i'\to\sigma_i)\right)\times P^{\rm A}(\sigma_1,\sigma_2,\ldots,\sigma_i',\ldots,\sigma_N;t). \quad (3)$$

Since the system is in contact with a heat bath at absolute temperature $T_{\rm A}$, each spin can change from σ_i to σ_i' in an unit time with the probability

$$W_i^{\rm A}(\sigma_i\to\sigma_i')=\frac{1}{\tau}\frac{\exp(-\beta\Delta E^{\rm A}(\sigma_i\to\sigma_i'))}{\sum_{\sigma_i'}\exp(-\beta\Delta E^{\rm A}(\sigma_i\to\sigma_i'))}, \quad (4)$$

where $\beta=1/k_{\rm B}T_{\rm A}$, $k_{\rm B}$ is the Boltzmann constant, the summation is over the six possible values $\pm5/2,\pm3/2,\pm1/2$ for σ_i', and

$$\Delta E^{\rm A}(\sigma_i\to\sigma_i') = -(\sigma_i'-\sigma_i)\left(J_1\sum_j S_j+J_2\sum_j\sigma_j+H\right) -({\sigma_i'}^2-\sigma_i^2)D \quad (5)$$

gives the change in the energy of the system when the σ_i spin changes. The $W_i^{\rm A}(\sigma_i\to\sigma_i')$ is given in Appendix A. The probabilities satisfy the detailed balance condition. Since $W_i^{\rm A}(\sigma_i\to\sigma_i')$ does not depend on the value of σ_i, we can write $W_i^{\rm A}(\sigma_i\to\sigma_i')=W_i^{\rm A}(\sigma_i')$, then the master equation becomes

$$\frac{\rm d}{{\rm d}t}P^{\rm A}(\sigma_1,\sigma_2,\ldots,\sigma_N;t) = -\sum_i\left(\sum_{\sigma_i\neq\sigma_i'}W_i^{\rm A}(\sigma_i')\right)P^{\rm A}(\sigma_1,\sigma_2,\ldots,\sigma_i,\ldots,\sigma_N;t) +\sum_i W_i^{\rm A}(\sigma_i)\left(\sum_{\sigma_i\neq\sigma_i'}P^{\rm A}(\sigma_1,\sigma_2,\ldots,\sigma_i',\ldots,\sigma_N;t)\right). \quad (6)$$

Since the sum of the probabilities is normalized to one, multiplying both sides of Eq. (6) by σ_k, taking the average, and finally using the mean-field approach, we obtain the first mean-field dynamic equation for the σ spins

$$\Omega\frac{\rm d}{{\rm d}\xi}m_\sigma=-m_\sigma+\frac{5\exp\left(2\frac{d}{T}\right)\sinh\left(\frac{5}{2}\frac{a_1}{T}\right)+3\exp\left(-2\frac{d}{T}\right)\sinh\left(\frac{3}{2}\frac{a_1}{T}\right)+\exp\left(-4\frac{d}{T}\right)\sinh\left(\frac{1}{2}\frac{a_1}{T}\right)}{2\exp\left(2\frac{d}{T}\right)\cosh\left(\frac{5}{2}\frac{a_1}{T}\right)+2\exp\left(-2\frac{d}{T}\right)\cosh\left(\frac{3}{2}\frac{a_1}{T}\right)+2\exp\left(-4\frac{d}{T}\right)\cosh\left(\frac{1}{2}\frac{a_1}{T}\right)}, \quad (7)$$

where $T=k_{\rm B}T_{\rm A}/|J_1|$, $d=D/|J_1|$, $a_1=(-z_1m_s+J_2/|J_1|z_2m_\sigma+h\cos(\xi))$, $h=H_0/|J_1|$, $m_\sigma=\langle\sigma\rangle$, $\xi=\omega t$, and $\Omega=\tau\omega$.

Now assuming that the σ spins on sublattice A remain momentarily fixed and the S spins on sublattice B change, we obtain the second mean-field dynamic equation by using a similar calculation

$$\Omega\frac{\rm d}{{\rm d}\xi}m_s=-m_s+\frac{5\exp\left(2\frac{d}{T}\right)\sinh\left(\frac{5}{2}\frac{a_2}{T}\right)+3\exp\left(-2\frac{d}{T}\right)\sinh\left(\frac{3}{2}\frac{a_2}{T}\right)+\exp\left(-4\frac{d}{T}\right)\sinh\left(\frac{1}{2}\frac{a_2}{T}\right)}{2\exp\left(2\frac{d}{T}\right)\cosh\left(\frac{5}{2}\frac{a_2}{T}\right)+2\exp\left(-2\frac{d}{T}\right)\cosh\left(\frac{3}{2}\frac{a_2}{T}\right)+2\exp\left(-4\frac{d}{T}\right)\cosh\left(\frac{1}{2}\frac{a_2}{T}\right)}, \quad (8)$$

where $m_s=\langle S\rangle$, and $a_2=(-z_1m_\sigma+J_3/|J_1|z_3m_s+h\cos(\xi))$. Hence, a set of mean-field dynamical equations of the system is obtained. We fixed $J_1=-1.0$, i.e., the intersublattice interaction is antiferromagnetic, and $\Omega=2\pi$. The solution and discussion of these equations are given in the next section.

3. Numerical results and discussion

3.1. Time variations of average sublattice magnetizations

In order to investigate the time variations of average sublattice magnetizations, first, we have to study the stationary solutions of the set of mean-field dynamic equations given by Eqs. (7) and (8) when the parameters T, J_2, J_3, d, and h are varied. The stationary solution of Eqs. (7) and (8) is a periodic function of ξ with period 2π, that is,

$$m_\sigma(\xi+2\pi)=m_\sigma(\xi), \quad (9a)$$

$$m_s(\xi+2\pi)=m_s(\xi). \quad (9b)$$

Moreover, they can be one of three types according to whether they have or not the following properties:

$$m_\sigma(\xi+\pi)=-m_\sigma(\xi), \quad (10a)$$

$$m_s(\xi+\pi)=-m_s(\xi). \quad (10b)$$

The first type of solution satisfies both Eqs. 10(a) and 10(b) and is called the symmetric solution. It corresponds to a paramagnetic (p) phase. In this solution, the average sublattice magnetizations $m_\sigma(\xi)$ and $m_s(\xi)$ are equal to each other. They oscillate around zero and are delayed with respect to the external magnetic field. The second type of solution, which does not satisfy Eqs. 10(a) and 10(b), is called the nonsymmetric solution and corresponds to an antiferromagnetic (af) phase. If $m_\sigma(\xi)$ and $m_s(\xi)$ oscillate

around $\pm 5/2$ and $\mp 5/2$, respectively, this solution is called the antiferromagnetic-5/2 ($\mathrm{af}_{5/2}$) phase; if $m_\sigma(\xi)$ and $m_s(\xi)$ oscillate around $\pm 3/2$ and $\mp 3/2$, respectively, this solution is called the antiferromagnetic-3/2 ($\mathrm{af}_{3/2}$) phase; if $m_\sigma(\xi)$ and $m_s(\xi)$ oscillate around $\pm 1/2$ and $\mp 1/2$, respectively, this solution is called the antiferromagnetic-1/2 ($\mathrm{af}_{1/2}$) phase. The third type of solution, which does not satisfy Eqs. 10(a) and 10(b), is called a nonsymmetric solution and corresponds to a ferrimagnetic (i) phase. In this case, $m_\sigma(\xi)$ and $m_s(\xi)$ are not equal to each other and oscillate around nonzero values. Hence, if $m_\sigma(\xi)$ and $m_s(\xi)$ oscillate around $\pm 5/2$ and $\mp 3/2$, respectively, this solution is called the ferrimagnetic-1 (i_1) phase; if $m_\sigma(\xi)$ and $m_s(\xi)$ oscillate around $\pm 5/2$ and $\mp 1/2$, respectively, this solution is called the ferrimagnetic-2 (i_2) phase; if $m_\sigma(\xi)$ and $m_s(\xi)$ oscillate around $\pm 3/2$ and $\mp 1/2$, respectively, this solution is called the ferrimagnetic-3 (i_3) phase. These facts can be seen explicitly by solving Eqs. (7) and (8) numerically. Equations (7) and (8) are solved by using the numerical method for a given set of parameters and initial values. A few explanatory examples are given in Fig. 2. Figures 2(a)–2(e) present the p, $\mathrm{af}_{5/2}$, and i_1 fundamental phases or solutions, and $\mathrm{i}_2+\mathrm{af}_{1/2}$ and $\mathrm{af}_{5/2}+\mathrm{af}_{3/2}+\mathrm{af}_{1/2}$ mixed phases, respectively. In addition to these three fundamental phases and two mixed phases, four more fundamental phases, namely, $\mathrm{af}_{3/2}$, $\mathrm{af}_{1/2}$, i_2, and i_3 fundamental phases, and eleven more mixed phases, namely, $\mathrm{af}_{5/2}+\mathrm{p}$ in which $\mathrm{af}_{5/2}$ and p solutions coexist, $\mathrm{af}_{1/2}+\mathrm{p}$ in which $\mathrm{af}_{1/2}$ and p solutions coexist, $\mathrm{i}_1+\mathrm{p}$ in which i_1 and p solutions coexist, $\mathrm{i}_2+\mathrm{p}$ in which i_2 and p solutions coexist, $\mathrm{i}_3+\mathrm{p}$ in which i_3 and p solutions coexist, $\mathrm{af}_{5/2}+\mathrm{af}_{1/2}$ in which $\mathrm{af}_{5/2}$ and $\mathrm{af}_{1/2}$ solutions coexist, $\mathrm{af}_{3/2}+\mathrm{af}_{1/2}$ in which $\mathrm{af}_{3/2}$ and $\mathrm{af}_{1/2}$ solutions coexist, $\mathrm{i}_1+\mathrm{af}_{1/2}$ in which i_1 and $\mathrm{af}_{1/2}$ solutions coexist, $\mathrm{i}_3+\mathrm{af}_{1/2}$ in which i_3 and $\mathrm{af}_{1/2}$ solutions coexist, $\mathrm{i}_1+\mathrm{i}_3+\mathrm{af}_{1/2}$ in which i_1, i_3, and $\mathrm{af}_{1/2}$ solutions coexist, the $\mathrm{i}_2+\mathrm{i}_3+\mathrm{af}_{1/2}$ in which i_2, i_3, and $\mathrm{af}_{1/2}$ solutions coexist, exist in the system.

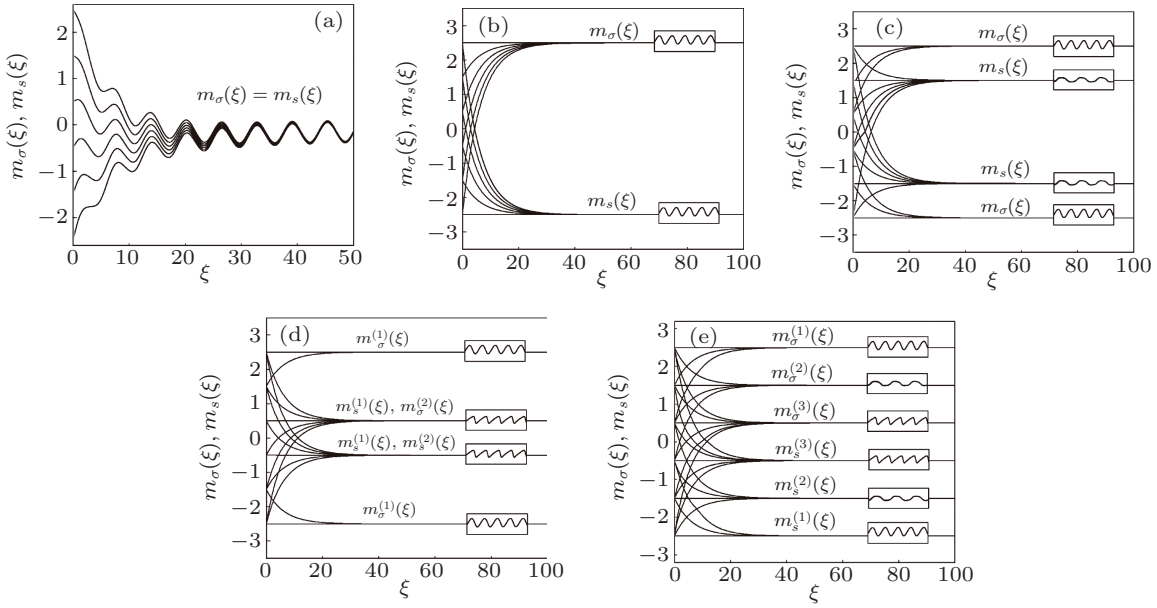


Fig. 2. Time variations of the average sublattice magnetizations $m_\sigma(\xi)$ and $m_s(\xi)$: (a) a paramagnetic phase (p) with $J_1 = -1.0$, $J_2 = 1.1$, $J_3 = 0.5$, $d = -3.5$, $h = 3.0$, and $T = 0.8$; (b) an antiferromagnetic-5/2 phase ($\mathrm{af}_{5/2}$) with, $J_1 = -1.0$, $J_2 = 1.1$, $J_3 = 0.1$, $d = 1.0$, $h = 0.1$, and $T = 0.1$; (c) a ferrimagnetic-1 phase (i_1) with $J_1 = -1.0$, $J_2 = 3.5$, $J_3 = 0.2$, $d = -4.0$, $h = 0.1$, and $T = 4.0$; (d) a coexistence region of ($\mathrm{i}_2+\mathrm{af}_{1/2}$) with $J_1 = -1.0$, $\mathrm{J}_2 = 7.5$, $J_3 = 0.1$, $d = -6.0$, $h = 0.2$, and $T = 2.0$; (e) a coexistence region of ($\mathrm{af}_{5/2}+\mathrm{af}_{3/2}+\mathrm{af}_{1/2}$) with $J_1 = -1.0$, $J_2 = 1.1$, $J_3 = 0.9$, $d = -2.7$, $h = 0.1$, and $T = 0.2$.

3.2. Thermal behavior of dynamic sublattice magnetizations and total magnetization

In this subsection, first, we investigate the behavior of the average sublattice magnetizations in a period (the dynamic sublattice magnetizations) as a function of the temperature. This investigation helps us to characterize the nature (first- or second-order) of the phase transitions and find the DPT points. Then, we study the dynamic total magnetization as a function of the temperature to find the dynamic compensation temperature and to determine the type of the dynamic compensation behavior. The dynamic sublattice magnetizations M_σ, M_s and the dynamic total magnetization $M_\mathrm{t} = (M_\sigma + M_s)/2$ are given by

$$M_\sigma = \frac{1}{2\pi}\int_0^{2\pi} m_\sigma(\xi)\,\mathrm{d}\xi, \tag{11a}$$

$$M_s = \frac{1}{2\pi}\int_0^{2\pi} m_s(\xi)\,\mathrm{d}\xi, \tag{11b}$$

$$M_\mathrm{t} = \frac{1}{2\pi}\int_0^{2\pi} \left(\frac{m_\sigma(\xi)+m_s(\xi)}{2}\right)\mathrm{d}\xi. \tag{11c}$$

The M_σ, M_s, and M_t as functions of the temperature for several values of interaction parameters are obtained by solving Eqs. 11(a)–11(c). The dynamic total magnetization M_t vanishes at the compensation temperature T_{comp}. Then, the compensation point can be determined by looking for the crossing point of the absolute values of the sublattice magnetizations. At the compensation point, we must have

$$\left|M_\sigma(T_{comp})\right| = \left|M_s(T_{comp})\right|, \tag{12}$$

$$\mathrm{sgn}\left[M_\sigma(T_{comp})\right] = -\mathrm{sgn}\left[M_s(T_{comp})\right]. \tag{13}$$

We also require that $T_{comp} < T_c$, where T_c is the critical point temperature. These conditions demonstrate that at T_{comp}, M_σ and M_s cancel each other, whereas at T_c both are zero. A few interesting examples are shown in Figs. 3(a)–3(e) to illustrate the calculation of the DPT points and the compensation temperatures. In these figures, T_c and T_t are the critical and the second- or the first-order phase transition temperatures, respectively. Figure 3(a) shows $|M_\sigma|$, $|M_s|$ and $|M_t|$ as functions of the temperature for $J_1 = -1.0$, $J_2 = 1.5$, $J_3 = 0.1$, $d = 1.0$, and $h = 0.1$. In Fig. 3(a), $|M_\sigma| = 2.5$ and $|M_s| = 2.5$ at zero temperature, and they decrease to zero continuously as the temperature increases until T_c, hence a second-order phase transition occurs at $T_c = 19.1$. In this case, the dynamic phase transition is from the $af_{5/2}$ phase to the p phase. Moreover, one compensation temperature exists in the system that exhibits the same behavior classified after the Néel theory[1] as the L type.[50] Figures 3(b) and 3(c) show $|M_\sigma|$, $|M_s|$, and $|M_t|$ as functions of the temperature for $J_1 = -1.0$, $J_2 = 1.1$, $J_3 = 0.5$, $d = -3.5$, $h = 0.3$ and two different initial values. The behavior shown in Fig. 3(b) is similar to that in Fig. 3(a); hence, the system undergoes a second-order phase transition at $T_c = 1.52$. In this case, the dynamic phase transition is from the $af_{1/2}$ phase to the p phase. Moreover, the compensation temperature or the L-type behavior occurs in the system again. In Fig. 3(c), the system undergoes two successive phase transitions. The first one is of first order, because the discontinuous occurs for the dynamic sublattice magnetizations at $T_t = 0.07$.

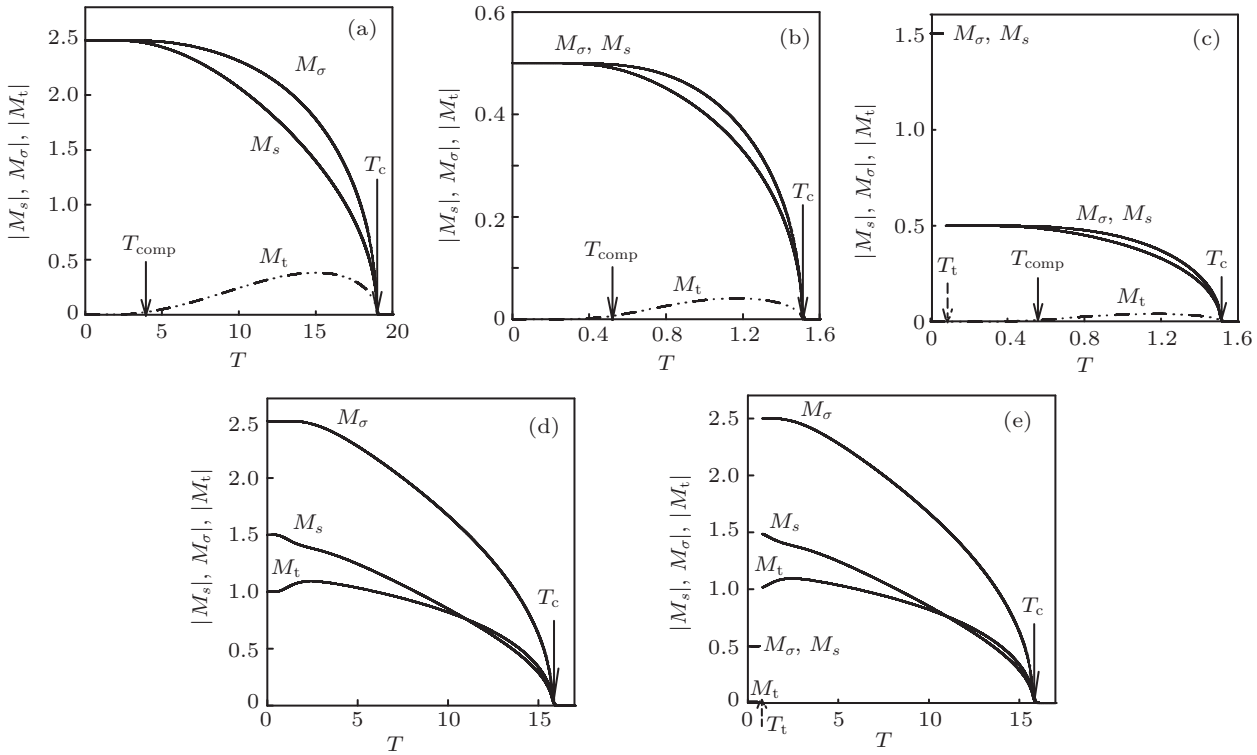


Fig. 3. The thermal behaviors of the dynamic sublattice magnetizations $|M_\sigma|$, $|M_s|$ and the dynamic total magnetization $|M_t|$. The T_c and T_t are the critical and the second- or the first-order phase transition temperatures, respectively. (a) Exhibiting a second-order phase transition from the $af_{5/2}$ phase to the p phase for $J_1 = -1.0$, $J_2 = 1.5$, $J_3 = 0.1$, $d = 1.0$, and $h = 0.1$, and T_c is found to be 19.1. (b) Exhibiting a second-order phase transition from the $af_{1/2}$ phase to the p phase for $J_1 = -1.0$, $J_2 = 1.1$, $J_3 = 0.5$, $d = -3.5$, and $h = 0.3$, and the initial values of $|M_\sigma|$ and $|M_s|$ are taken as 0.5; T_c is found to be 1.52. (c) Exhibiting two successive phase transitions, the first one is a first-order phase transition from the $af_{3/2}$ phase to the $af_{1/2}$ phase, and the second one is a second-order phase transition from the $af_{1/2}$ phase to the p phase for $J_1 = -1.0$, $J_2 = 1.1$, $J_3 = 0.5$, $d = -3.5$, and $h = 0.3$, and the initial values of $|M_\sigma|$ and $|M_s|$ are taken as 1.5; T_t and T_c are found to be 0.07 and 1.52, respectively. (d) Exhibiting a second-order phase transition from the i_1 phase to the p phase for $J_1 = -1.0$, $J_2 = 4.0$, $J_3 = 0.5$, $d = -4.1$, and $h = 6.5$, and the initial values of $|M_\sigma|$ and $|M_s|$ are taken as 2.5 and 1.5, respectively; T_c is found to be 15.9. (e) Exhibiting two successive phase transitions, the first one is a first-order phase transition from the $af_{1/2}$ phase to the i_1 phase and the second one is a second-order phase transition from the i_1 phase to the p phase for $J_1 = -1.0$, $J_2 = 4.0$, $J_3 = 0.5$, $d = -4.1$, and $h = 6.5$, and the initial values of $|M_\sigma|$ and $|M_s|$ are taken as 0.5; T_t and T_c are found to be 0.7 and 15.9, respectively.

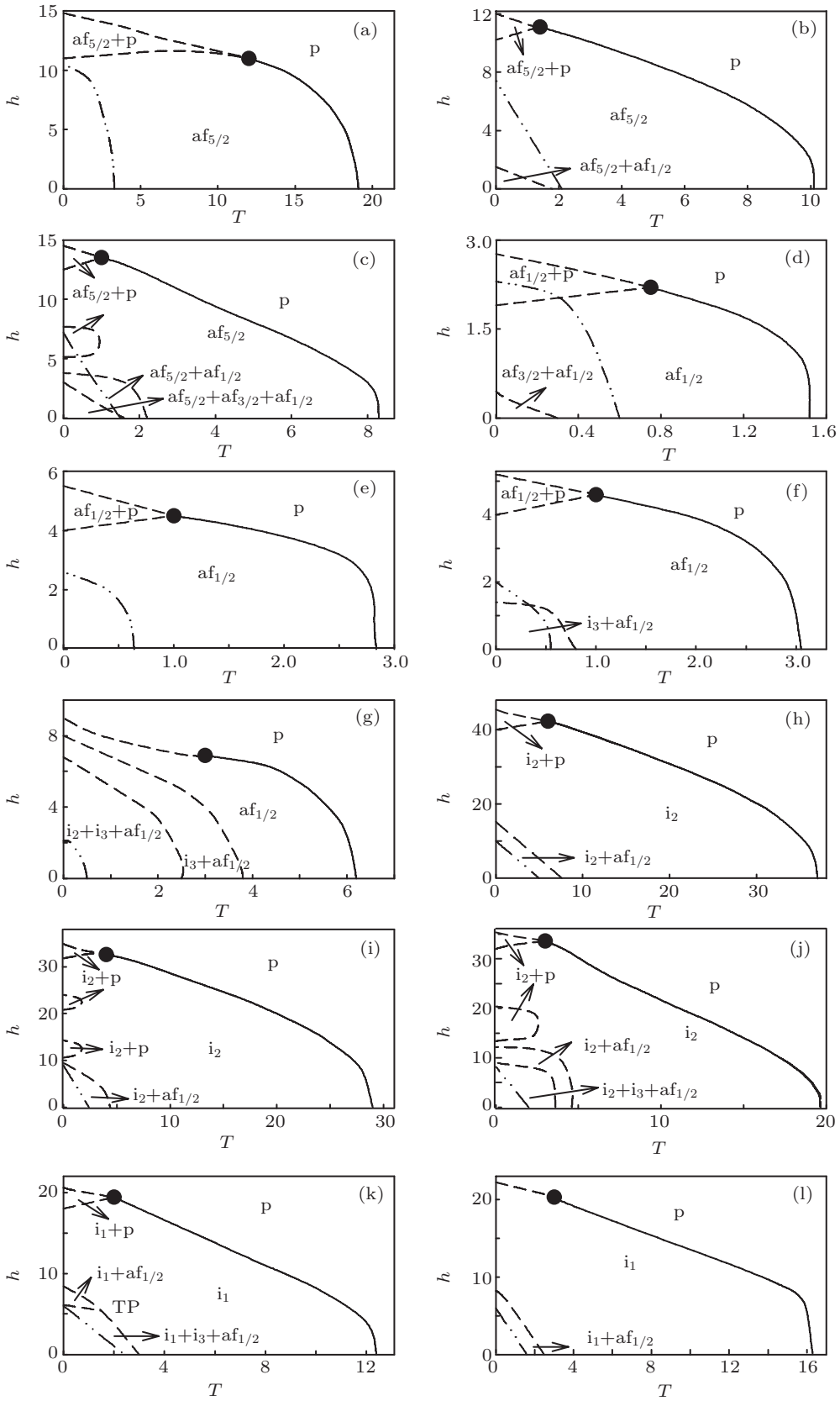


Fig. 4. (color online) Dynamic phase diagrams (including the dynamic compensation temperatures) of the kinetic spin-5/2 Ising system in the (T,h) plane. Dashed and solid lines are the dynamic first- and second-order phase boundaries, respectively. The dash-dot-dot line illustrates the compensation temperatures. The special points are the dynamic tricritical point with the filled circle (•) and the dynamic triple point (TP). (a) $J_1 = -1.0$, $J_2 = 1.5$, $J_3 = 0.1$, $d = 1.0$; (b) $J_1 = -1.0$, $J_2 = 1.1$, $J_3 = 0.1$, $d = -1.9$; (c) $J_1 = -1.0$, $J_2 = 1.1$, $J_3 = 0.9$, $d = -2.7$; (d) $J_1 = -1.0$, $J_2 = 1.1$, $J_3 = 0.5$, $d = -3.5$; (e) $J_1 = -1.0$, $J_2 = 5.0$, $J_3 = 0.9$, $d = -10.0$, (f) $J_1 = -1.0$, $J_2 = 5.0$, $J_3 = 0.9$, $d = -7.0$; (g) $J_1 = -1.0$, $J_2 = 9.0$, $J_3 = 0.3$, $d = -10.0$, (h) $J_1 = -1.0$, $J_2 = 10.0$, $J_3 = 0.1$, $d = -8.0$; (i) $J_1 = -1.0$, $J_2 = 7.5$, $J_3 = 0.1$, $d = -6.0$; (j) $J_1 = -1.0$, $J_2 = 7.0$, $J_3 = 0.1$, $d = -7.0$; (k) $J_1 = -1.0$, $J_2 = 3.5$, $J_3 = 0.2$, $d = -4.0$; (l) $J_1 = -1.0$, $J_2 = 4.0$, $J_3 = 0.5$, $d = -4.1$.

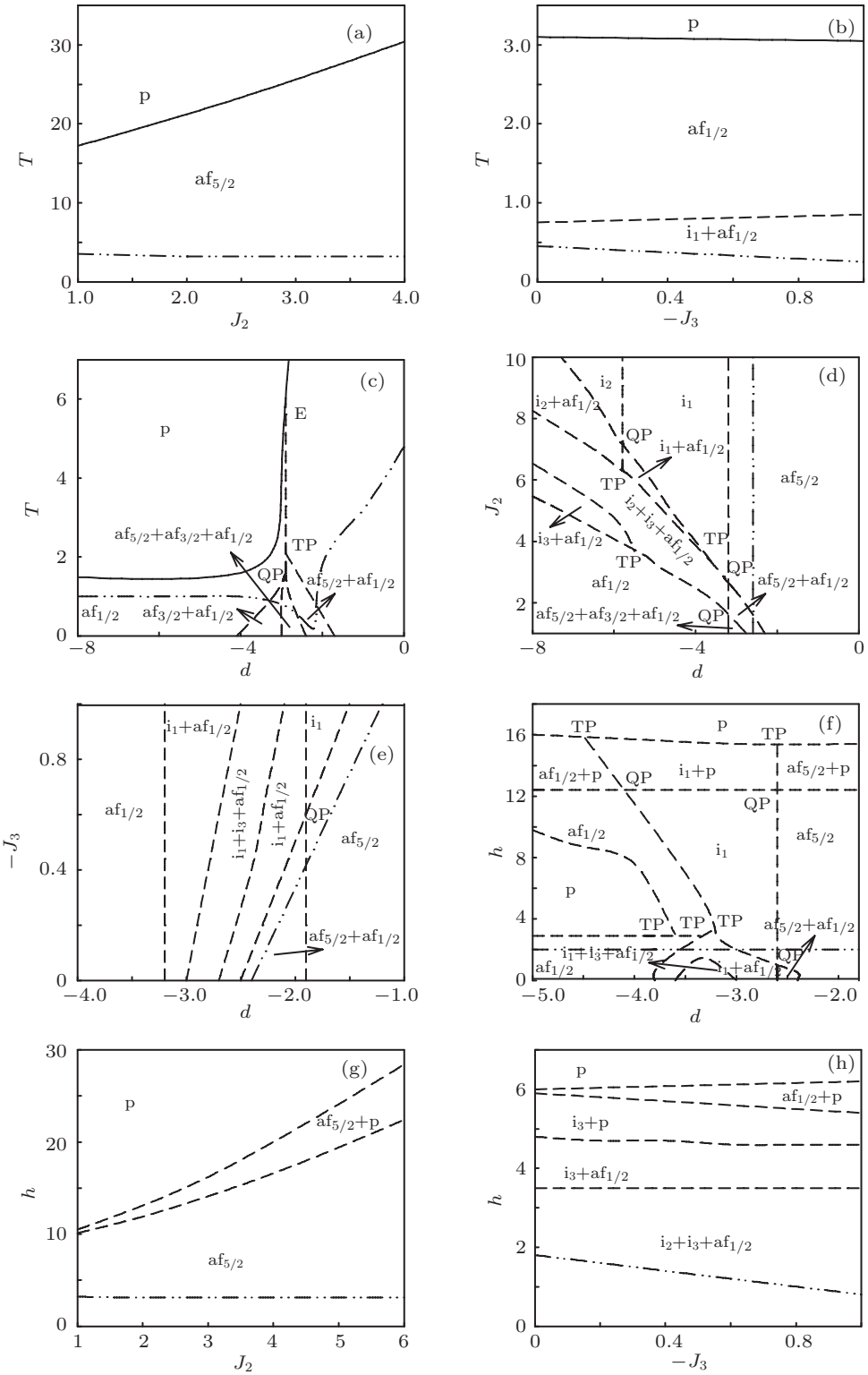


Fig. 5. Dynamic phase diagrams in different planes, where TP, QP, and E are the dynamic triple point, the dynamic quadruple point, and dynamic critical end point, respectively. (a) In (J_2,T) plane for $J_1=-1.0$, $J_3=0.1$, $h=1.0$, and $d=1.0$; (b) in $(-J_3,T)$ plane for $J_1=-1.0$, $J_2=1.4$, $h=0.1$, and $d=-3.1$; (c) in (d,T) plane for $J_1=-1.0$, $J_2=1.1$, $J_3=0.9$, and $h=0.1$; (d) in (d,J_2) plane for $J_1=-1.0$, $J_3=0.6$, $h=0.9$, and $T=0.5$; (e) in $(d,-J_3)$ plane for $J_1=-1.0$, $J_2=1.5$, $h=0.1$, and $T=0.1$; (f) in (d,h) plane for $J_1=-1.0$, $J_2=2.0$, $J_3=0.2$, and $T=0.1$; (g) in (J_2,h) plane for $J_1=-1.0$, $J_3=0.2$, $d=-1.0$, and $T=1.2$; (h) in $(-J_3,h)$ plane for $J_1=-1.0$, $J_2=6.0$, $d=-7.0$, and $T=1.0$.

The transition is from the $af_{3/2}$ phase to the $af_{1/2}$ phase. The second one is a second-order phase transtion from the $af_{1/2}$ phase to the p phase at $T_c=1.52$. From Figs. 3(b) and 3(c), we can see that the $af_{3/2}+af_{1/2}$ mixed phase exists until T_t, and this fact is also shown in the phase diagram of Fig. 4(d) explicitly. Figures 3(d) and 3(e) show $|M_\sigma|$, $|M_s|$, and $|M_t|$ as functions of the temperature for $J_1=-1.0$, $J_2=4.0$, $J_3=0.5$, $d=-4.1$, and $h=6.5$. In Fig. 3(d), $|M_\sigma|=2.5$ and $|M_s|=1.5$ at zero temperature, and they decrease to zero continuously as the temperature increases until T_c, hence a second-order phase

transition occurs at $T_c = 15.90$. In this case, the dynamic phase transition is from the i_1 phase to the p phase. In Fig. 3(e), the system undergoes two successive phase transitions. The first one is of first order, because the discontinuous occurs for the dynamic sublattice magnetizations at $T_t = 0.70$. The transition is from the $af_{1/2}$ phase to the i_1 phase. The second one is a second-order phase transtion from the i_1 phase to the p phase at $T_c = 15.90$. This means that the coexistence region, i.e., the $i_1 + af_{1/2}$ mixed phase, exists in the system until T_t. There is no compensation temperature in the system for this case.

3.3. Dynamic phase diagrams

Since we have obtained the DPT points and the compensation temperatures, we can now present the dynamic phase diagrams of the system. The calculated dynamic phase diagrams, including the dynamic compensation temperatures, in the (T,h) plane are presented in Fig. 4, and one explanatory phase diagram for each of the (J_2,T), $(-J_3,T)$, (d,T), (d,J_2), $(d,-J_3)$, (d,h), (J_2,h), and $(-J_3,h)$ planes is presented in Fig. 5 for different values of the interaction parameters. In these dynamic phase diagrams, the dashed, the solid, and the dash-dot-dot lines represent the first-order, the second-order phase transition temperatures, and the compensation temperature, respectively. The dynamic tricritical point is denoted by a filled circle. In the (T,h) plane, twelve main topological different types of dynamic phase diagrams are found and presented in Fig. 4. From these phase diagrams, the following phenomena have been observed. (i) All phase diagrams contain the dynamic compensation temperature. (ii) These dynamic phase diagrams exhibit one dynamic tricritical point. (iii) The system contains the p, $af_{5/2}$, $af_{3/2}$, $af_{1/2}$, i_1, i_2, and i_3 fundamental phases and the $af_{5/2} + p$, $af_{1/2} + p$, $i_1 + p$, $i_2 + p$, $i_3 + p$, $af_{5/2} + af_{1/2}$, $af_{3/2} + af_{1/2}$, $i_1 + af_{1/2}$, $i_2 + af_{1/2}$, $i_3 + af_{1/2}$, $af_{5/2} + af_{3/2} + af_{1/2}$, $i_1 + i_3 + af_{1/2}$, and $i_2 + i_3 + af_{1/2}$ mixed phases. (iv) Figure 4(k) displays the dynamic triple point (TP) where three phases (i_1, $i_1 + af_{1/2}$, $i_1 + i_3 + af_{1/2}$) or solutions coexist. (v) The dynamic phase boundaries among the fundamental phases are mostly second-order phase transition lines, but among the mixed phases or between the fundamental and the mixed phases are the first-order phase transition lines. It is worthwhile to mention that a phase diagram similar to Figs. 4(a) and 4(e) was also obtained in the kinetic mixed spin-1 and spin-2 Ising system.[31] The phase diagrams shown in Figs. 4(b)–4(d) and 4(f)–4(l) are only observed in this system.

We calculate the dynamic phase diagrams, including the compensation temperatures, in the (J_2,T), $(-J_3,T)$, (d,T), (d,J_2), $(d,-J_3)$, (d,h), (J_2,h), and $(-J_3,h)$ planes, and six, eleven, six, four, three, three, five, and nine main topological different types of dynamic phase diagrams are found, respectively. From these phase diagrams, one explanatory dynamic phase diagram for each of these planes is given in Figs. 5(a)–5(h). The basic properties of these phase diagrams are given as follows. (i) All phase diagrams contain the dynamic compensation temperature. (ii) The dynamic phase diagrams in the (d,T), (d,J_2), and (d,h) planes exhibit one, three, and five dynamic TPs, respectively. (iii) The dynamic phase diagrams in the (d,T), (d,J_2), and (d,h) planes exhibit one, three, and three dynamic quadruple points (QP) where four solutions or phases coexist, respectively. (iv) In Fig. 5(c), the dynamic phase diagram displays the dynamic critical end point (E). We should also mention that we do observe a phase diagram in Fig. 5(a) which is very similar to that found in the earlier studies of the mixed Ising systems with spins (1/2, 1),[26] spins (1/2, 3/2),[27] spins (1, 3/2),[29] spins (2, 5/2),[30] and spins (1, 2).[31] Moreover, a phase diagram similar to that in Fig. 5(b) has also been obtained in the kinetic mixed spin-1 and spin-2 Ising system,[31] but the $i_1 + af_{1/2}$ mixed phase becomes the af + p mixed phase. Figures 5(c)–5(h) are new phase diagrams, which were not obtained in kinetic Ising systems.[26–31]

4. Summary and conclusion

In this work, we have analyzed with a mean-field approach the stationary states of the kinetic spin-5/2 Ising model with bilinear and crystal-field interactions under the presence of a time-varying oscillating external magnetic field on alternate layers of a hexagonal lattice. The model consists of two interpenetrating sublattices with $\sigma = 5/2$ and $S = 5/2$. The model includes intersublattice, intrasublattice, and crystal-field interactions and a sinusoidal magnetic field. We use the Glauber-type stochastic dynamics to describe the time evolution of the system. We have studied the time variations of the average sublattice magnetizations in order to find the phases of the system and the thermal behavior of the average sublattice magnetizations in a period (the dynamic sublattice magnetizations) to obtain the dynamic phase transition (DPT) points as well as to characterize the nature (first- or second-order) of the transitions. The dynamic total magnetization is investigated as a function of the temperature to find the dynamic compensation temperature and to determine the type of the dynamic compensation behavior. Finally, dynamic phase diagrams, including compensation temperatures, are presented in the (T,h), (J_2,T), $(-J_3,T)$, (d,T), (d,J_2), $(d,-J_3)$, (d,h), (J_2,h), and $(-J_3,h)$ planes for different values of the interaction parameters. The dynamic

phase diagrams contain seven different fundamental phases $(\mathrm{p}, \mathrm{af}_{5/2}, \mathrm{af}_{3/2}, \mathrm{af}_{1/2}, \mathrm{i}_1, \mathrm{i}_2, \mathrm{i}_3)$, thirteen different mixed phases which are binary and ternary combinations of the fundamental phases. The system displays the dynamic tricritical point, the dynamic triple point, the dynamic quadruple point, and the dynamic critical end point depending on the interaction parameters. Moreover, in general, the dynamic boundary between the fundamental phases is a second-order line, but the boundary between the fundamental and the mixed phases, and also the boundaries among the mixed phases are first-order phase transition lines. From these investigations, we deduce that although phase diagrams similar to those in Figs. 4(a), 4(e), 5(a), and 5(b) have been obtained in the kinetic of mixed systems with different spins.[26,27,29–31] Figures 4(b)–4(d), 4(f)–4(l), and 5(c)–5(h) show new phase diagrams that have been obtained only in this kinetic Ising system.

We compare the present results with the results of the kinetic spin-1 Ising system[51] on a hexagonal lattice. (i) Both systems display the L-type behavior. (ii) The kinetic spin-5/2 Ising system contains seven fundamental phases besides thirteen different mixed phases, but the kinetic spin-1 Ising system contains two fundamental phases besides two mixed phases. (iii) The kinetic spin-5/2 Ising system exhibits the dynamic TP, the dynamic QP, and the dynamic E, but the kinetic spin-1 Ising system does not. (iv) The kinetic spin-5/2 Ising system has more topological different phase diagrams than the kinetic spin-1 Ising system.

Finally, it is worthwhile to mention that some of the first-order phase transition lines as well as the dynamic special points might be artifact of the mean-field approach due to its limitations, such as the correlation of spin fluctuation has not been considered. However, this study suggests that the kinetic spin-5/2 Ising system on alternate layers of a hexagonal lattice has an interesting dynamic behavior and gives rich dynamic phase diagrams. Hence, we hope that our detailed theoretical investigation may stimulate further works to study the DPT points and the compensation temperatures, and present the dynamic phase diagrams in the mixed Ising model by using more accurate techniques such as dynamic Monte–Carlo simulations and the renormalization group calculations. Moreover, our results will be instructive in the time-comsuming process of searching the critical behavior of this system while using the dynamic MC simulations, they may also shed some light on the experimentel work.

Appendix A: Values of $W_i^{\mathrm{A}}(\sigma_i \to \sigma_i')$

$$
\begin{aligned}
W_i^{\mathrm{A}}\left(\frac{3}{2}\to\frac{5}{2}\right) &= W_i^{\mathrm{A}}\left(\frac{1}{2}\to\frac{5}{2}\right) = W_i^{\mathrm{A}}\left(-\frac{1}{2}\to\frac{5}{2}\right) = W_i^{\mathrm{A}}\left(-\frac{3}{2}\to\frac{5}{2}\right) = W_i^{\mathrm{A}}\left(-\frac{5}{2}\to\frac{5}{2}\right) \\
&= \frac{1}{\tau}\frac{\exp(2\beta D)\exp\left(\dfrac{5\beta x}{2}\right)}{2\exp(2\beta D)\cosh\left(\dfrac{5\beta x}{2}\right)+2\exp(-2\beta D)\cosh\left(\dfrac{3\beta x}{2}\right)+2\exp(-4\beta D)\cosh\left(\dfrac{\beta x}{2}\right)}, \\
W_i^{\mathrm{A}}\left(\frac{5}{2}\to\frac{3}{2}\right) &= W_i^{\mathrm{A}}\left(\frac{1}{2}\to\frac{3}{2}\right) = W_i^{\mathrm{A}}\left(-\frac{1}{2}\to\frac{3}{2}\right) = W_i^{\mathrm{A}}\left(-\frac{3}{2}\to\frac{3}{2}\right) = W_i^{\mathrm{A}}\left(-\frac{5}{2}\to\frac{3}{2}\right) \\
&= \frac{1}{\tau}\frac{\exp(-2\beta D)\exp\left(\dfrac{3\beta x}{2}\right)}{2\exp(2\beta D)\cosh\left(\dfrac{5\beta x}{2}\right)+2\exp(-2\beta D)\cosh\left(\dfrac{3\beta x}{2}\right)+2\exp(-4\beta D)\cosh\left(\dfrac{\beta x}{2}\right)}, \\
W_i^{\mathrm{A}}\left(\frac{5}{2}\to\frac{1}{2}\right) &= W_i^{\mathrm{A}}\left(\frac{3}{2}\to\frac{1}{2}\right) = W_i^{\mathrm{A}}\left(-\frac{1}{2}\to\frac{1}{2}\right) = W_i^{\mathrm{A}}\left(-\frac{3}{2}\to\frac{1}{2}\right) = W_i^{\mathrm{A}}\left(-\frac{5}{2}\to\frac{1}{2}\right) \\
&= \frac{1}{\tau}\frac{\exp(-4\beta D)\exp\left(\dfrac{\beta x}{2}\right)}{2\exp(2\beta D)\cosh\left(\dfrac{5\beta x}{2}\right)+2\exp(-2\beta D)\cosh\left(\dfrac{3\beta x}{2}\right)+2\exp(-4\beta D)\cosh\left(\dfrac{\beta x}{2}\right)}, \\
W_i^{\mathrm{A}}\left(\frac{5}{2}\to-\frac{1}{2}\right) &= W_i^{\mathrm{A}}\left(\frac{3}{2}\to-\frac{1}{2}\right) = W_i^{\mathrm{A}}\left(\frac{1}{2}\to-\frac{1}{2}\right) = W_i^{\mathrm{A}}\left(-\frac{3}{2}\to-\frac{1}{2}\right) = W_i^{\mathrm{A}}\left(-\frac{5}{2}\to-\frac{1}{2}\right) \\
&= \frac{1}{\tau}\frac{\exp(-4\beta D)\exp\left(-\dfrac{\beta x}{2}\right)}{2\exp(2\beta D)\cosh\left(\dfrac{5\beta x}{2}\right)+2\exp(-2\beta D)\cosh\left(\dfrac{3\beta x}{2}\right)+2\exp(-4\beta D)\cosh\left(\dfrac{\beta x}{2}\right)},
\end{aligned}
$$

$$W_i^{\mathrm{A}}\left(\frac{5}{2}\to-\frac{3}{2}\right)=W_i^{\mathrm{A}}\left(\frac{3}{2}\to-\frac{3}{2}\right)=W_i^{\mathrm{A}}\left(\frac{1}{2}\to-\frac{3}{2}\right)=W_i^{\mathrm{A}}\left(-\frac{1}{2}\to-\frac{3}{2}\right)=W_i^{\mathrm{A}}\left(-\frac{5}{2}\to-\frac{3}{2}\right)$$
$$=\frac{1}{\tau}\frac{\exp(-2\beta D)\exp\left(-\dfrac{3\beta x}{2}\right)}{2\exp(2\beta D)\cosh\left(\dfrac{5\beta x}{2}\right)+2\exp(-2\beta D)\cosh\left(\dfrac{3\beta x}{2}\right)+2\exp(-4\beta D)\cosh\left(\dfrac{\beta x}{2}\right)},$$
$$W_i^{\mathrm{A}}\left(\frac{5}{2}\to-\frac{5}{2}\right)=W_i^{\mathrm{A}}\left(\frac{3}{2}\to-\frac{5}{2}\right)=W_i^{\mathrm{A}}\left(\frac{1}{2}\to-\frac{5}{2}\right)=W_i^{\mathrm{A}}\left(-\frac{1}{2}\to-\frac{5}{2}\right)=W_i^{\mathrm{A}}\left(-\frac{3}{2}\to-\frac{5}{2}\right)$$
$$=\frac{1}{\tau}\frac{\exp(2\beta D)\exp\left(-\dfrac{5\beta x}{2}\right)}{2\exp(2\beta D)\cosh\left(\dfrac{5\beta x}{2}\right)+2\exp(-2\beta D)\cosh\left(\dfrac{3\beta x}{2}\right)+2\exp(-4\beta D)\cosh\left(\dfrac{\beta x}{2}\right)}.$$

References

[1] Néel L 1948 *Ann. Phys.* **3** 137
[2] Mansuripur M 1987 *J. Appl. Phys.* **61** 1580
[3] Mathoniere C, Nuttall C J, Carling S G and Day P 1996 *Inorg. Chem.* **35** 1201
[4] Hernando A and Kulik T 1994 *Phys. Rev. B* **49** 7064
[5] Kaneyoshi T 1995 *Solid State Commun.* **93** 691
[6] Abubrig O F, Bobák A, Horváth D and Jaščur M 2002 *Czech. J. Phys.* **52** 131
[7] Machado E and Buendía G M 2003 *Phys. Rev. B* **68** 224411
[8] Boechat B, Filgueiras R A, Cordeiro C and Branco N S 2002 *Physica A* **304** 429
[9] Buendía G M and Cardona W 1999 *Phys. Rev. B* **59** 6784
[10] Oitmaa J 2005 *Phys. Rev. B* **72** 224404
[11] Benayad N, Lahcini T and Fathi A 2007 *Condens. Matter* **8** 33
[12] Bobák A and Jaščur M 1995 *Phys. Rev. B* **51** 11533
[13] Kaneyoshi T, Jaščur M and Tomczak P 1992 *J. Phys.: Condens. Matter* **4** L653
[14] Bobák A, Jaščur M, Horváth D and Balcerzak T 2002 *Czech. J. Phys.* **52** 127
[15] Jiang W, Wei G and Zhang Z 2003 *Phys. Rev. B* **68** 134432
[16] Buendía G M and Novotny M A 1997 *J. Phys.: Condens. Matter* **9** 5951
[17] Albayrak E 2007 *Physica B Condens. Matter* **391** 47
[18] Ekiz C and Erdem R 2006 *Phys. Lett. A* **352** 291
[19] Buendía G M and Liendo J A 1997 *J. Phys.: Condens. Matter* **9** 5439
[20] Aydiner E, Yüksel Y, Kış E and Polat H 2009 *J. Magn. Magn. Mater.* **321** 3193
[21] Kaneyoshi T 1989 *Solid State Commun.* **70** 975
[22] Espriella N De La and Buendía G M 2011 *J. Phys.: Condens. Matter* **23** 176003
[23] Ekiz C 2006 *J. Magn. Magn. Mater.* **307** 139
[24] Godoy M, Leite V S and Figueiredo W 2004 *Phys. Rev. B* **69** 054428
[25] Figueiredo W, Godoy M and Leite V S 2004 *Braz. J. Phys.* **34** 392
[26] Keskin M and Ertaş M 2010 *J. Stat. Phys.* **139** 333
[27] Keskin M, Deviren B and Canko O 2009 *IEEE Trans. Mag.* **45** 2640
[28] Deviren B and Keskin M 2010 *J. Stat. Phys.* **140** 934
[29] Keskin M and Kantar E 2010 *J. Magn. Magn. Mater.* **322** 2789
[30] Keskin M and Ertaş M 2009 *Phys. Rev. E* **80** 061140
[31] Korkmaz T and Temizer Ü 2012 *J. Magn. Magn. Mater.* **324** 3876
[32] Plascak J A, Moreira J G and sá Barreto F C 1993 *Phys. Lett. A* **173** 360
[33] Kaneyoshi T and Jaščur M 1993 *Phys. Sta. Sol. B* **175** 225
[34] Benyoussef A 1993 *Phys. Sta. Sol. B* **178** 233
[35] Kerouad M, Saber M and Tucker J W 1994 *Physica A* **210** 424
[36] Song W J and Yang C Z 1994 *Solid State Commun.* **92** 361
[37] Lee Y S, Greven M, Wells B O, Birgeneau B J and Shirane G 1998 *Eur. Phys. J. B* **5** 15
[38] He Z, Ueda Y and Itoh M 2007 *Solid State Commun.* **141** 22
[39] Cowley R A, Aharony A, Birgeneau R J, Pelcovits R A, Shirane G and Thurston T R 1993 *Zeitschrift fuer Phys. B* **93** 5
[40] Cowley R A, Shirane G, Birgeneau R J and Guggenheim H J 1977 *Phys. Rev. B* **15** 4292
[41] Costa B V and Pires A S T 2003 *J. Magn. Magn. Mater.* **262** 316
[42] Christianson R J, Leheny R L, Birgeneau R J and Erwin R W 2001 *Phys. Rev. B* **63** 140401
[43] Wildes A R, Rønnow H M, Roeesli B, Haris M J and Godfrey K W 2006 *Phys. Rev. B* **74** 094422
[44] Deviren B, Keskin M and Canko O 2009 *Phase Trans.* **82** 683
[45] Ertaş M and Keskin M 2010 *Phase Trans.* **83** 349
[46] Glauber R J 1963 *J. Math. Phys.* **4** 294
[47] Ertaş M, Keskin M and Deviren B 2012 *J. Magn. Magn. Mater.* **324** 1503
[48] Chern G, Horng L, Shieh W K and Wu T C 2001 *Phys. Rev. B* **63** 094421
[49] Kageyama H, Khomskii D I, Levitin R Z and Vasil'ev A N 2003 *Phys. Rev. B* **67** 224422
[50] Chikazumi S 1997 *Physics of Ferromagnetism* (Oxford: Oxford University Press)
[51] Temizer Ü, Keskin M and Canko O 2009 *J. Magn. Magn. Mater.* **321** 2999